Computing and Informatics, Vol. 45, 2026, 1183–1207, doi: 10.31577/cai_2026_5_1183

RESEARCH ON INDOOR POSITIONING ALGORITHM BASED ON UWB TECHNOLOGY AT FIRE SCENE

Chongyu Wang

School of Aerospace Engineering
Xiamen University
No. 4221 Xiangan South Road
Xiamen, China
e-mail: 34520222201096@stu.xmu.edu.cn

Xuhui Que, Defa Kong

Pen-Tung Sah Institute of Micro-Nano Science and Technology
Xiamen University
No. 4221 Xiangan South Road
Xiamen, China
e-mail: {35120221151673, 19920231151647}@stu.xmu.edu.cn

Juan Liu*

Pen-Tung Sah Institute of Micro-Nano Science and Technology
Xiamen University
No. 4221 Xiangan South Road
Xiamen, China
e-mail: cecyliu@xmu.edu.cn

Abstract. Aiming at the positioning problem of dynamically deployed temperature and smoke sensors in intelligent fire protection systems, an ultra-wideband (UWB) positioning method was applied. This led to the design of a dynamically deployed sensor that integrates temperature and smoke sensing, positioning, and

* Corresponding author

wireless communication functions. The adaptive obstacle compensation trilateral measurement algorithm and nonlinear least squares compensation were used to achieve accurate positioning in harsh fire environments. Experiments show that in complex indoor environments, when the number of partition walls on a single coordinate axis does not exceed 3, the positioning error can be within 3 cm. The sensor can also obtain the on-site temperature and smoke distribution in real time.

Keywords: UWB positioning, fire, fire rescue, positioning algorithm, nonlinear optimization

Mathematics Subject Classification 2010: 93E10

1 INTRODUCTION

For firefighting and rescue, real-time acquisition of on-site temperature and smoke distribution can provide the best decision support for evacuation and rescue. Therefore, modern intelligent firefighting systems need to incorporate dynamically deployed environmental parameter sensors. These sensors should not only detect temperature and smoke parameters but also achieve precise positioning. Additionally, these sensors wirelessly transmit positioning and environmental data to the back-end system. The back-end system then uses prediction algorithms to determine the real-time distribution and development trends of temperature and smoke parameters, supporting evacuation and rescue decisions. The main design challenge of dynamically deployed environmental parameter sensors is to achieve accurate positioning in harsh fire environments. For outdoor fires, GPS and Beidou systems are usually used to achieve high-precision positioning. However, the research challenges of indoor fires are huge. On the one hand, the indoor GPS signal is too weak to achieve accurate positioning; on the other hand, the indoor environment is complex, and the fire conditions are extremely harsh, so traditional positioning methods (e.g. WiFi) are ineffective.

At present, multiple research teams are conducting in-depth research on indoor positioning. Shang and Wang [1] reviewed WiFi fingerprinting-based indoor positioning, while Liu et al. [2] surveyed WiFi-based indoor positioning techniques. In 2019, Abbas et al. from Alexandria University proposed a deep learning-based indoor positioning system WiDeep [3] in their paper, which can achieve centimeter-level positioning through deep neural network data processing. In the same year, Yu et al. proposed a new non-line-of-sight (NLOS) cancellation algorithm [4], which significantly improved the accuracy and reliability of indoor UWB positioning systems by modeling UWB signals. However, both methods require complex modeling of the signal transmission environment, which does not meet the requirements of rapid deployment of indoor fire positioning.

In 2018, Sadowski and Spachos from the University of Guelph used RSSI (received signal strength indicator) for indoor positioning in the paper "RSSI-Based Indoor Localization with the Internet of Things" [5], and achieved high-precision positioning based on existing Wi-Fi signals. However, under the harsh and complex conditions of the fire scene, Wi-Fi positioning may fail. In addition, since RSSI positioning is affected by shadows, multipath effects, etc., its accuracy in indoor positioning is often insufficient. In the same year, Wang et al. from Nanjing University of Aeronautics and Astronautics studied indoor positioning based on UWB ranging technology [6]. They established a positioning system using UWB signals and proposed an improved sliding average filtering algorithm to reduce the impact of UWB signal fluctuations. However, this method consumes a lot of bandwidth, seriously affects the information transmission at the fire scene, and is not suitable for harsh and complex environments.

Other studies have explored correction, optimization, and fitting methods for wireless positioning. He et al. [7] investigated a correction and compensation triangulation positioning algorithm based on RSSI. Wang et al. [8] studied a Bluetooth positioning method based on least squares. Li et al. [9] compared numerical fitting methods for fingerprint curves and investigated their optimization.

Due to the harsh conditions at the fire scene, indoor fire positioning must be resistant to high temperatures and can be deployed quickly. In addition, there are many obstacles indoors, and conventional positioning methods are difficult to achieve sufficient accuracy, which requires that the indoor positioning method used must maintain high accuracy in complex environments. UWB positioning technology can not only achieve centimeter-level accuracy, but also has low energy consumption and strong anti-interference ability. At present, UWB technology is widely used in conventional indoor positioning and complex environments such as mines. Considering the complexity of the fire scene environment and the requirements of high precision and rapid deployment, UWB is more suitable for positioning in fire scenes than other technologies. Hao et al. [10] investigated UWB-based indoor coplanar localization and anchor placement optimization. Li et al. [11] reviewed collaborative positioning methods for swarms using vision, LiDAR, and wireless sensors.

In a fire scene, multiple wireless sensing nodes (for temperature, smoke, CO_2, etc.) are deployed, and their precise 3D spatial coordinates are obtained through integrated positioning technologies (such as UWB combined with WiFi RSSI). The positioning results serve as the foundation for constructing the spatial distribution of the fire environment. They provide essential coordinate support for subsequent tasks such as map rendering and dynamic modeling of the sensed data. Based on this, a temporary, multi-node dynamically deployed environmental perception system can better assist firefighting operations and achieve higher-density operations. It can also deploy measurements when conventional perception fails, form real-time rescue decision-making plans, and effectively assist rescue and evacuation through temperature, smoke calculations, and fire development predictions.

2 DESIGN OF THE POSITIONING DEVICE

2.1 Analysis of Requirements for Fire Scene Positioning Devices

Fire scenes often present harsh conditions, including heavy smoke that can interfere with the normal operation of positioning devices. Additionally, the high temperatures at these sites necessitate the use of heat-resistant and stable components whenever possible. Moreover, fire environments are inherently complex and unstable, with risks such as fire spread and structural collapse. Therefore, positioning devices must be designed to withstand these challenging conditions and ensure reliable performance.

2.2 Circuit Design of the Positioning Device

This system uses the DW1000 chip to enable high-precision positioning. Its key advantages – high accuracy, compact size, and low power consumption – make it particularly suitable for emergency scenarios such as fire rescue. The microcontroller, using USART communication, receives distance data from positioning tags to various base stations. A 4G communication module then transmits this data to the backend for centralized processing.

2.2.1 Configuration of the STM32 Microcontroller System

The STM32 microcontroller operates at frequencies of up to 72 MHz, delivering high computational speed and real-time performance while integrating various peripheral modules. Additionally, it is designed to function in harsh environments and features efficient power management, supporting multiple standby modes to minimize energy consumption.

From a technical standpoint, the STM32 microcontroller meets the requirements for self-localization and temperature acquisition devices in fire scenes. Its efficient data acquisition and processing capabilities, combined with extensive peripheral support, enable it to connect to multiple sensors simultaneously. This allows for the collection and processing of critical data such as temperature and distance.

UWB technology is a wireless communication method, which is known for its high-precision positioning capabilities. It is widely used in the Internet of Things (IoT) and high-accuracy localization applications. Compared to traditional positioning technologies such as GPS, Wi-Fi, and Bluetooth, UWB offers superior accuracy and strong anti-interference performance. This makes it ideal for dense deployment scenarios and harsh environments. The schematic of the DW1000 chip used in the positioning module is shown in Figure 1.

When selecting a UWB positioning module, factors such as ease of secondary development, cost-effectiveness, and portability were carefully considered. The chosen module, based on the DW1000 chip, enables high-precision positioning and supports short-range networks with multiple nodes. It features low power consumption, fast

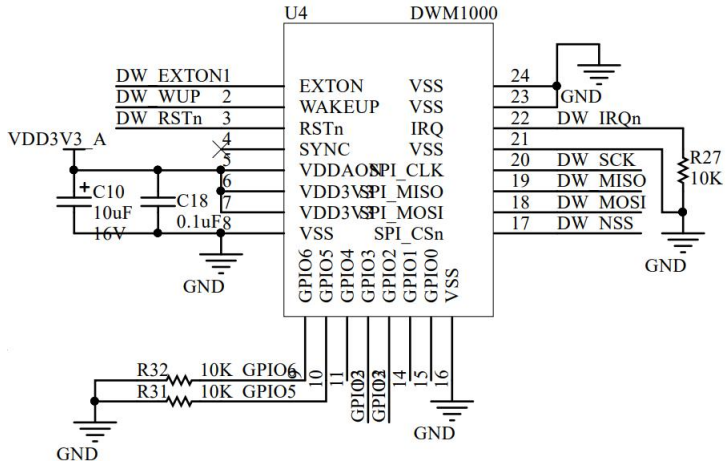


Figure 1. Schematic diagram of the DW1000 chip

startup, and adaptability to various applications, with the flexibility to develop custom intelligent hardware programs as needed. The circuit schematic of the UWB positioning module is shown in Figure 2.

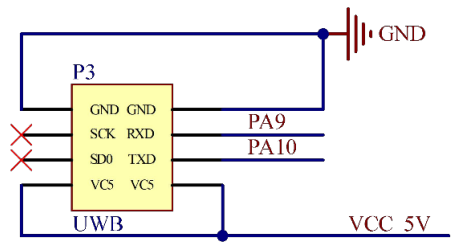


Figure 2. Schematic diagram of the UWB positioning module

2.2.2 Circuit Design of the 4G Module

To ensure efficient transmission of collected data to the backend for unified processing, a 4G module is integrated into the device. This module offers fast response times, low power consumption, and high reliability. Its compact size contributes to a lightweight design, making it well-suited for mobile applications. Additionally, a 4G module capable of functioning reliably in harsh environments was selected to meet the demanding conditions of fire scenes.

2.2.3 Circuit Board Design and Production

Figure 3 shows the actual physical image of the main control board, which connects various modules in the self-localization temperature acquisition device. These include the positioning tag module and the OLED display module. This device was developed to validate the feasibility and accuracy of the algorithm. The breadboard circuit features a double-layer routing design with a two-layer board structure. Its layout optimizes space utilization, with strategically arranged components to enhance efficiency and functionality.



Figure 3. Photograph of the positioning device

3 POSITIONING PROGRAM DESIGN

3.1 Positioning Method Based on Triangulation

The DWM1000 chip used in this experiment measures distances using the Time of Flight (TOF) method to achieve precise positioning. This approach offers high accuracy, and UWB technology itself is highly resistant to interference, making it less susceptible to environmental disturbances. However, it also has limitations, particularly in complex environments with multiple semi-enclosed or fully enclosed walls. In these cases, electromagnetic wave transmission is affected by various factors, resulting in increased delays and greater measurement errors. Therefore, in practical applications, parameter adjustments are necessary to maintain algorithm accuracy and robustness under different conditions.

As illustrated in Figure 4, the DWM1000 employs a bidirectional ranging method to determine the distance between the tag and the base station. The process involves the tag sending a signal to the base station, which, upon receiving it, transmits a reply signal back to the tag. This exchange involves four-time nodes: T1, T2, T3, and T4, where T1 and T4 are recorded on the tag's timestamp, while T2 and T3 are on the base station's timestamp. The formula for distance calculation is as follows:

$$2T_S = (T_4 - T_1) - (T_3 - T_2). \tag{1}$$

This formula can be used to calculate the two-way flight time, which in turn allows for the calculation of distance using the following formula as follows:

$$D = T_S \times c. \tag{2}$$

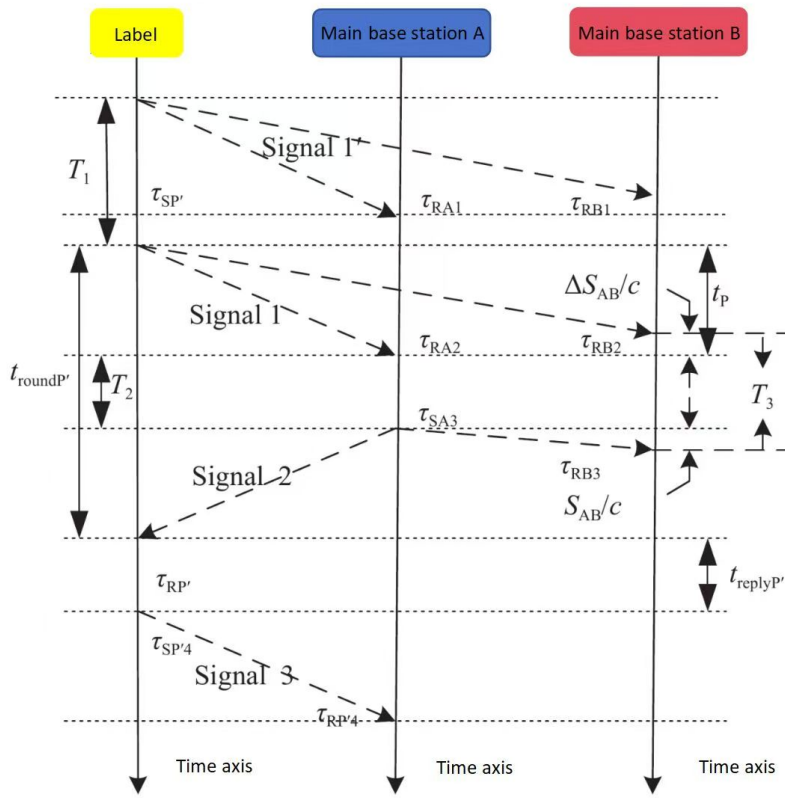


Figure 4. Schematic diagram of two-way ranging

After determining the distances from the tag to each base station using this method, triangulation can be applied to calculate the tag's coordinates. Due to environmental variations, the specific coordinates of the base stations must be input before localization. The tag's coordinates can then be derived using the corresponding formula.

As shown in Figure 5, assume there are three base stations – A, B, and C – and a tag, O. The known coordinates of A, B, and C are (X_a, Y_a), (X_b, Y_b), and (X_c, Y_c), respectively. Let the coordinates of tag O be (X, Y), with its distances to A, B, and C denoted as d_a, d_b, and d_c, respectively.

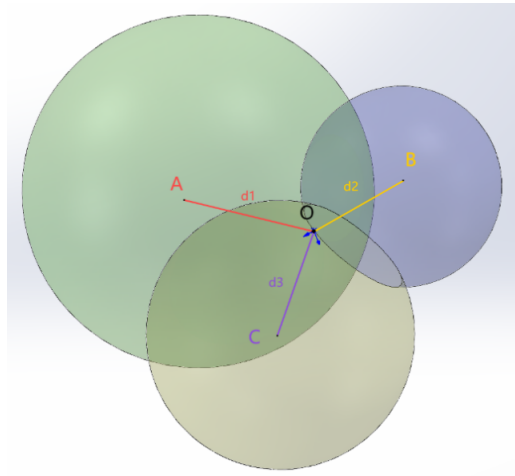


Figure 5. Schematic diagram of the triangulation method

By creating the following equations:

$$\begin{cases} \sqrt{(X-X_a)^2+(Y-Y_a)^2+(Z-Z_a)^2} = d_a, \\ \sqrt{(X-X_b)^2+(Y-Y_b)^2+(Z-Z_b)^2} = d_b, \\ \sqrt{(X-X_c)^2+(Y-Y_c)^2+(Z-Z_c)^2} = d_c. \end{cases} \tag{3}$$

We can derive the coordinates of O as follows:

$$\begin{pmatrix} X \\ Y \\ Z \end{pmatrix} = \begin{bmatrix} X_a - X_b & Y_a - Y_b & Z_a - Z_b \\ X_a - X_c & Y_a - Y_c & Z_a - Z_c \end{bmatrix}^{-1} \begin{bmatrix} \frac{(d_a^2-d_b^2)-(X_a^2-X_b^2)-(Y_a^2-Y_b^2)-(Z_a^2-Z_b^2)}{2} \\ \frac{(d_a^2-d_c^2)-(X_a^2-X_c^2)-(Y_a^2-Y_c^2)-(Z_a^2-Z_c^2)}{2} \end{bmatrix}. \tag{4}$$

Using this algorithm, the UWB positioning device performs initial localization and determines approximate coordinates, which lays the foundation for further experiments and the development of refined equations.

3.2 Coordinate Calculation Method

In the positioning system, the UWB positioning module functions as the tag. To determine the tag's position, the first step is to obtain the coordinate values of the known base stations and retrieve the distances from each base station to the tag from storage. These distances are then used to calculate the three-dimensional coordinates of the tag through triangulation.The data reception process is summarized in Figure 6.

Under ideal conditions, the triangulation formula can be directly applied to calculate the tag's coordinates. However, due to environmental interference and

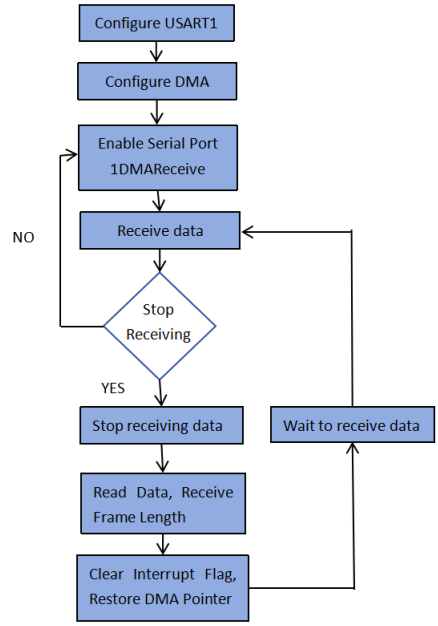


Figure 6. Data reception process flowchart

device-related factors, the measured distances often deviate from the ideal values. As a result, the spheres centered at the three base stations, with radii equal to their respective distances to the tag, may not intersect perfectly at a single point. Therefore, a specialized algorithm is required to estimate an ideal position, providing the best solution for the current self-localizing device coordinates.

When four base stations are involved in localization, the fourth base station (A_3) typically serves as an auxiliary. Assuming the four base stations are A_0, A_1, A_2, and A_3, the ranging data from the first three base stations (A_0, A_1, A_2) can produce two possible coordinate solutions: result1 and result2. To identify the correct coordinates, the ranging information from A_3 is used. Specifically, the distances from result1 and result2 to the sphere defined by A_3 are calculated, and the solution nearest to the sphere is selected as the final optimal solution. This approach effectively reduces ambiguity and improves positioning accuracy. These steps are typically implemented in a function called GetLocation, with the detailed flow shown in Figure 7. This ensures stability and precision in the results through clear calculation steps.

3.3 Algorithm Revision

After completing the programming of the positioning model, it is necessary to calibrate and debug it. Based on the working environment of the device, the debugging

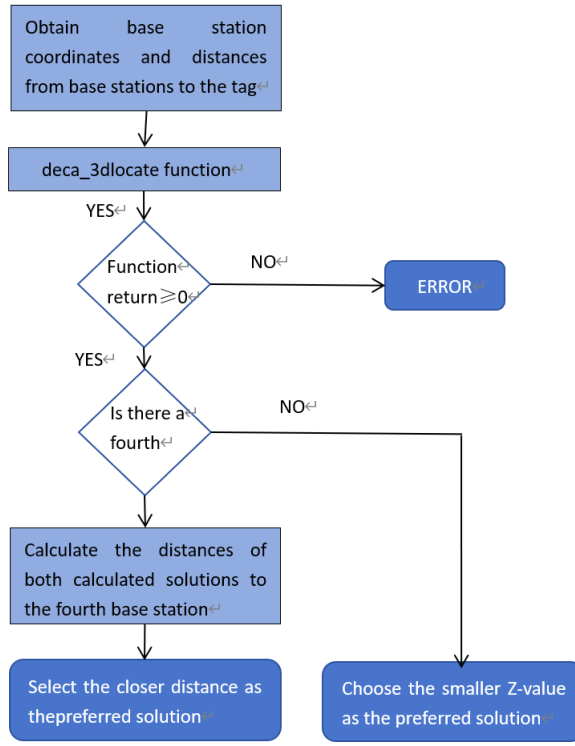


Figure 7. Coordinate calculation flowchart

was conducted in an indoor space, resulting in the following calibration formulas:

$$\begin{cases} X_{\text{actual}} = 0.98 \times X_{\text{measured}} + 0.11, \\ Y_{\text{actual}} = 0.83 \times Y_{\text{measured}} + 0.32, \\ Z_{\text{actual}} = -0.14 \times Z_{\text{measured}} + 1.44. \end{cases} \tag{5}$$

Assuming that the actual value of the X-axis coordinate is (X), the measured value of the X-axis coordinate is (X_1), the number of partition walls on the X-axis is (X_M), and the number of semi-partition walls is (X_N); the actual value of the Y-axis coordinate is (Y), the measured value of the Y-axis coordinate is (Y_1), the number of partition walls on the Y-axis is (Y_M), and the number of semi-partition walls is (Y_N).

Based on the experimental data and curve fitting, it was found that the overall slope of the fitted curve showed little difference. The differences were observed only in the intercepts. Therefore, it is possible to process the slope data to derive the corresponding formula, allowing us to input the respective numbers of semi-partition

walls and partition walls to obtain the corresponding formula. The fitting results yield the model:

$$\begin{cases} X = 0.76X_1 + 0.13X_M - 0.04X_N + 0.57, \\ Y = 0.86Y_1 + 0.22Y_M - 0.02Y_N + 0.41. \end{cases} \tag{6}$$

The final experiment showed that the positioning accuracy of the device can reach centimeter-level precision. This is mainly due to the use of UWB technology, which inherently provides high accuracy and is capable of centimeter-level positioning in open environments. However, in indoor settings, the presence of numerous obstacles significantly reduces positioning accuracy. By improving the algorithm to mitigate the effects of NLOS conditions, centimeter-level positioning was successfully achieved.

The specific experimental and analysis process will be presented in detail in the next section.

4 UWB DEVICE POSITIONING EXPERIMENT

4.1 Calibration and Debugging of the Positioning Module

Due to the diverse and complex application environments of UWB in various firefighting scenarios, the positioning module is influenced by factors such as temperature, latitude, longitude, and air quality. These factors can cause discrepancies between the measured and actual values. To achieve more accurate localization, calibration and debugging of the module are necessary.

The calibration experiment was conducted within an 8.4 m × 4.2 m test region inside a 9.0 m × 6.211 m office. Figure 8 shows the office layout and the boundary of the test region. It is furnished with various desks and chairs, without partition walls, to simulate a practical application scenario while ensuring no interference with future improvements.

The four base stations are positioned at the corners of the testing area using tripods. The line between base stations 0 and 1 serves as the X-axis, while the line between base stations 0 and 2 serves as the Y-axis, establishing a coordinate system. The heights of the base stations above the ground are 1.5 m, 1.4 m, 1.6 m, and 1.8 m, respectively. A handheld tag is moved to various locations within the test area to record its estimated coordinates. After taking three measurements at each position, the average value is calculated, compared to the actual coordinates, and then fitted for calibration. The positioning error distribution before calibration is shown in Figure 9. The corresponding contour plot is presented in Figure 10.

Before calibration, the maximum absolute errors for the X, Y, and Z coordinates are 0.21 m, 0.69 m, and 1.58 m, respectively. These results satisfy the basic requirement of a positioning error of less than ±2 m, achieving meter-level localization.

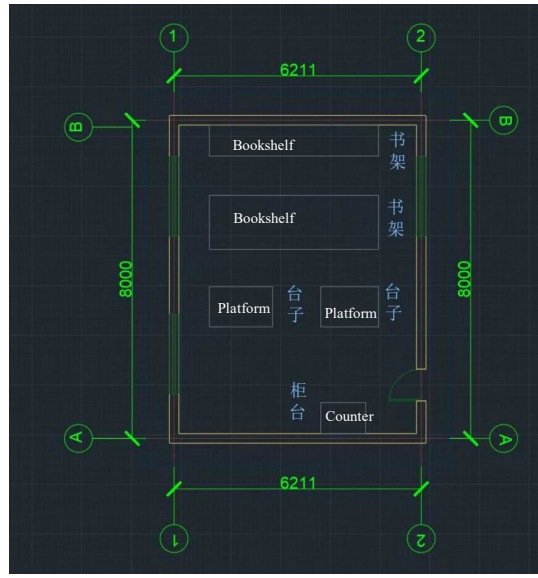


Figure 8. Calibration testing area

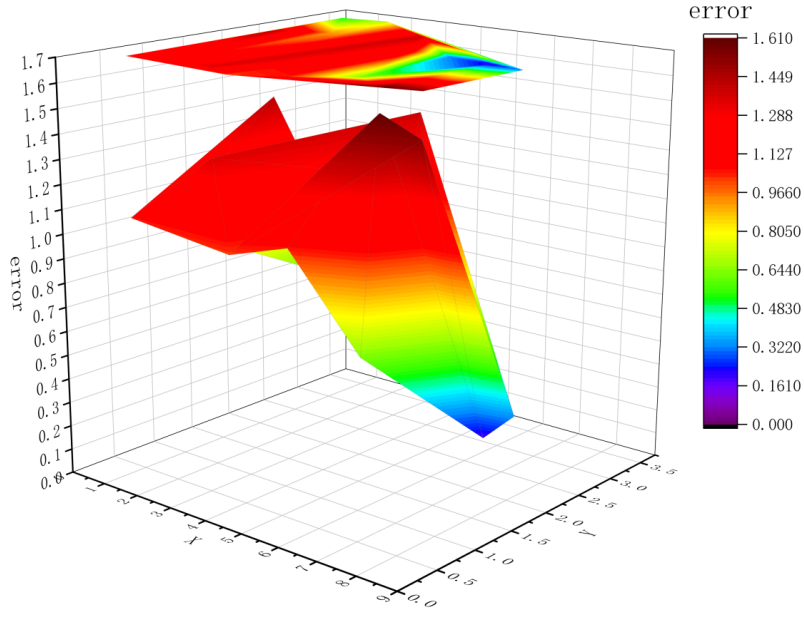


Figure 9. Error distribution image before calibration

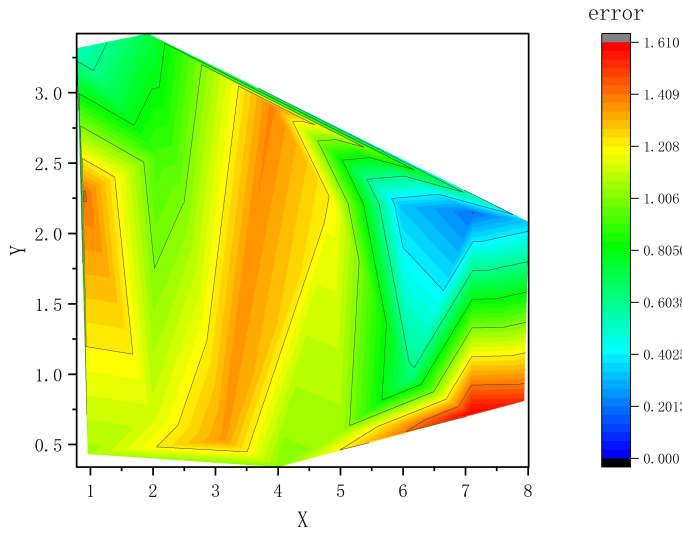


Figure 10. Contour plot of error distribution before calibration

Fitting the measured coordinates to the reference coordinates yields the following calibration formulas:

$$\begin{cases} X_{\text{actual}} = 0.98 \times X_{\text{measured}} + 0.11, \\ Y_{\text{actual}} = 0.83 \times Y_{\text{measured}} + 0.32, \\ Z_{\text{actual}} = -0.14 \times Z_{\text{measured}} + 1.44. \end{cases} \tag{7}$$

After calibrating the positioning module, additional experiments were conducted at the site shown in Figure 11.

The positioning error distribution after calibration and its contour plot are shown in Figures 12 and 13, respectively.

After calibration, the maximum absolute errors for the X, Y, and Z coordinates are reduced to 0.08 m, 0.05 m, and 0.05 m, respectively. Therefore, when site conditions allow, calibration should be performed prior to localization to substantially reduce errors.

4.2 Positioning Data and Obstacle Model

When signals propagate under NLOS conditions, the transmitted signal may reach the receiver through paths such as penetration, reflection, or diffraction. This results in increased propagation time and reduced signal strength, which can affect distance calculations. Although the UWB positioning device, after calibration, achieves centimeter-level accuracy in the absence of concrete wall obstructions, it

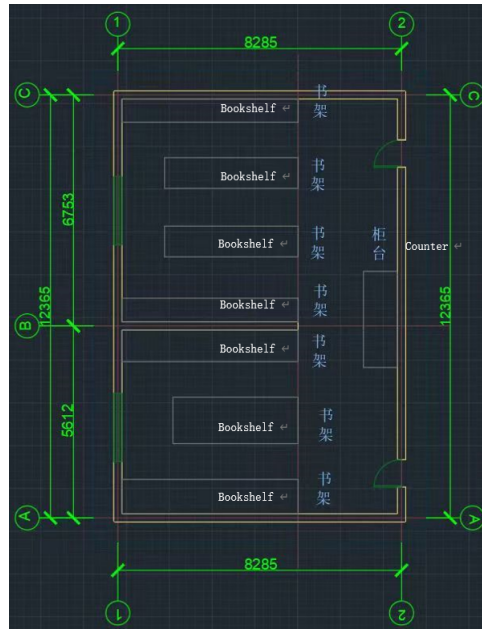


Figure 11. Experimental site for verification after calibration

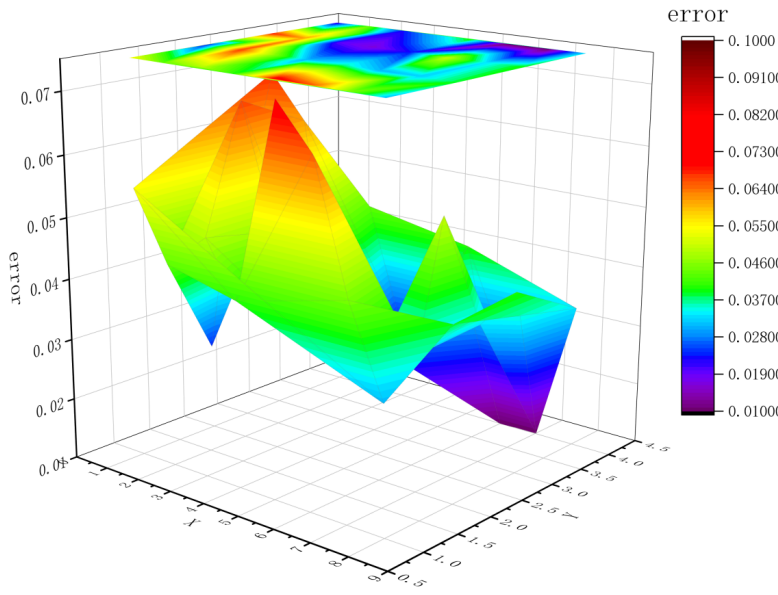


Figure 12. Error distribution image after calibration

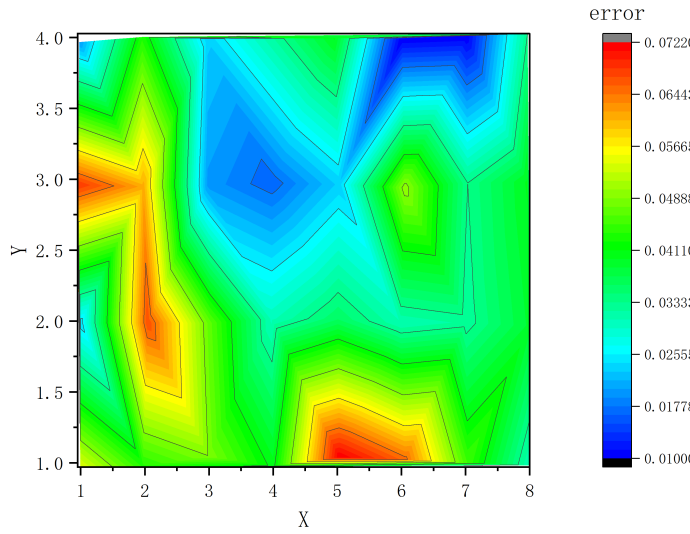


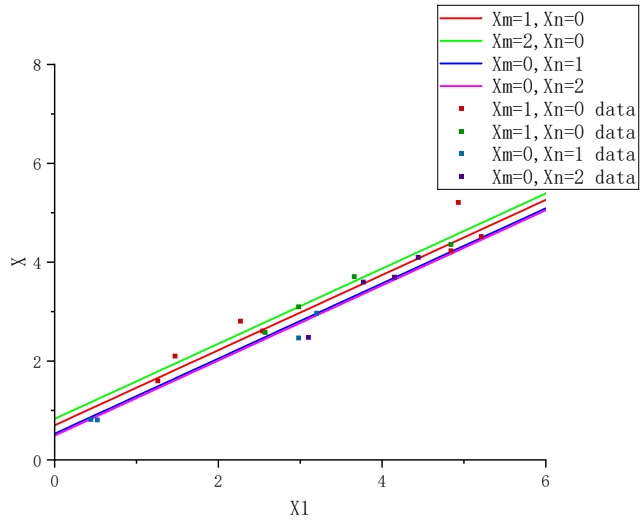
Figure 13. Contour plot of error distribution after calibration

still encounters significant errors when confronted with semi-partitioned or fully partitioned concrete obstacles. These situations require corresponding algorithmic corrections.

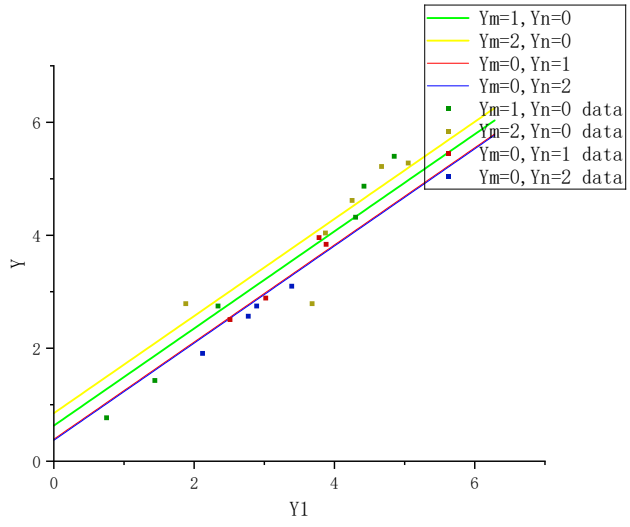
Yu et al. [4] investigated NLOS mitigation for UWB localization in harsh indoor environments. Sui et al. [12] investigated UWB NLOS recognition in LiDAR point clouds and an indoor fusion positioning algorithm.

The experiments indicated that concrete walls affect the positioning accuracy of the UWB module. This study uses experimental data to construct an empirical coordinate correction model for the tested wall configurations. Let the actual value of the X-axis coordinate be (X), the measured value of the X-axis coordinate be (X_1), the number of partition walls on the X-axis be (X_M), and the number of semi-partition walls on the X-axis be (X_N). Similarly, let the actual value of the Y-axis coordinate be (Y), the measured value of the Y-axis coordinate be (Y_1), the number of partition walls on the Y-axis be (Y_M), and the number of semi-partition walls on the Y-axis be (Y_N). The experimental data and fitted curves for the X and Y coordinates in the presence of concrete walls are shown in Figure 14.

By fitting the experimental data, it was observed that the overall slope of the fitting curve shows minimal distinction, with differences primarily at the ends. As a result, corresponding formulas can be derived by processing the slope data. These formulas allow for the input of the relevant counts of semi-partition and partition walls to generate the corresponding results. The equations can be solved using the



a) X-Axis



b) Y-Axis

Figure 14. Experimental data and curve fitting in the presence of concrete walls

lsqnonlin function, yielding the following model:

$$\begin{cases} X = 0.76X_1 + 0.13X_M - 0.04X_N + 0.57, \\ Y = 0.86Y_1 + 0.22Y_M - 0.02Y_N + 0.41. \end{cases} \tag{8}$$

Experimental tests were conducted to evaluate the effectiveness of the model. A rectangular area measuring 7 m in length and 5 m in width was used, with base stations positioned at the four corners.Various environments were selected for the experiments to assess the model's performance under complex conditions, as shown in Figure 15. The line between base stations 0 and 1 serves as the X-axis, and the line between base stations 0 and 2 serves as the Y-axis, establishing the coordinate system. After distance calibration, experimental measurements of the positioning data were collected.

Figures 16 and 17 show the positioning error distributions along the X and Y axes, respectively, after applying the obstacle compensation model.

Table 1 summarizes the mean positioning errors and their standard deviations along the X and Y axes before and after obstacle compensation.

	Mean signed error		**Standard deviation**	
	X	**Y**	**X**	**Y**
Before compensation	0.036	0.053	0.397	0.303
After compensation	0.028	−0.003	0.073	0.149

Table 1. Positioning errors and standard deviations before and after compensation (Unit: m)

Thus, it can be concluded that after establishing the error correction model, both the average error and standard deviation are significantly reduced. This results in centimeter-level positioning accuracy. When concrete walls obstruct signal transmission during firefighting operations, the software parameters can be adjusted to correct errors and mitigate the impact of NLOS on positioning.

5 FIRE SCENE TEMPERATURE MONITORING USING THE POSITIONING DEVICE

Temperature sensors were added to the experimental device, and the same field used in the error correction experiment was selected, with air conditioning activated for temperature measurement. The temperature distribution map of the experimental site is shown in Figure 18.

By integrating the positioning device with the temperature measurement system, a comprehensive temperature distribution map of the entire room was created. In the event of a fire, the device can generate real-time temperature contour maps of the scene. This aids firefighting efforts and helps predict fire spread trends.

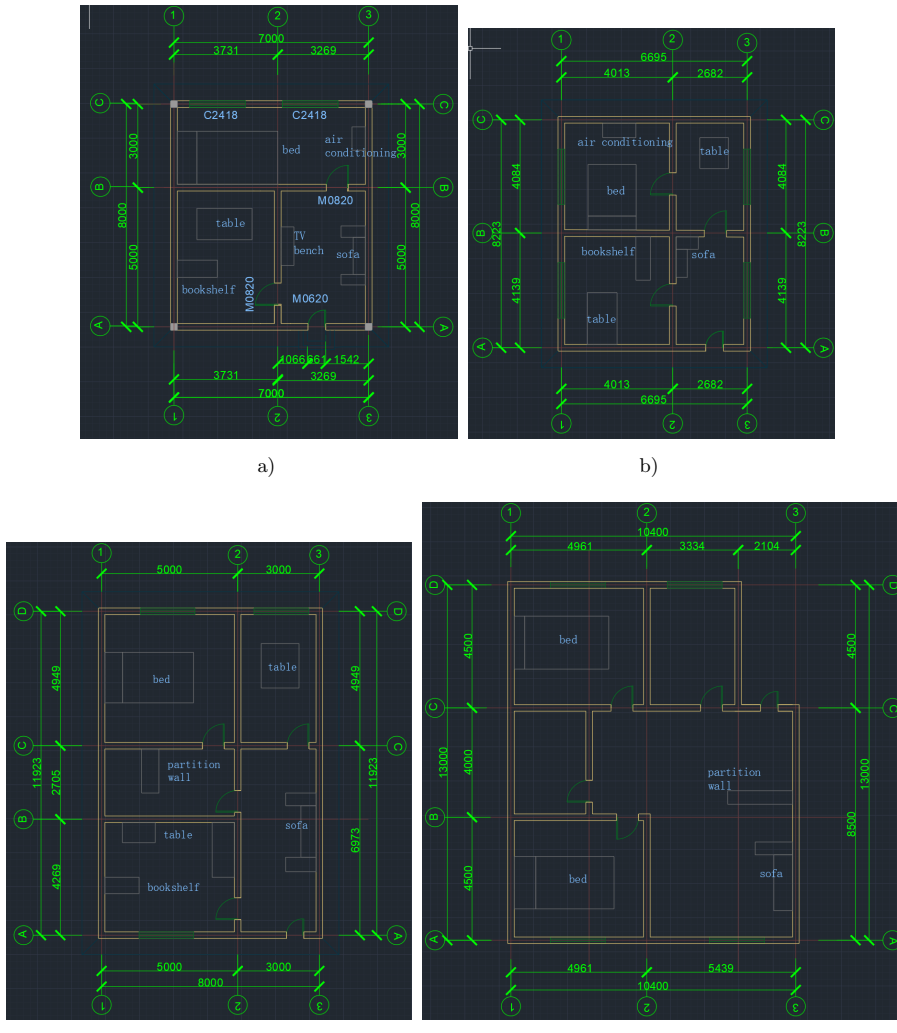


Figure 15. Experimental site structure diagram

Additionally, this enables the development of a dynamically deployable, multi-node fire environment perception system.

Figure 19 illustrates the system visualization of the temperature and smoke distribution fields.

By further deploying multiple wireless sensing nodes (for temperature, smoke, CO_2, etc.), it is possible to bind parameter data with spatial locations. This facilitates the construction of spatio-temporal distribution maps for temperature, smoke,

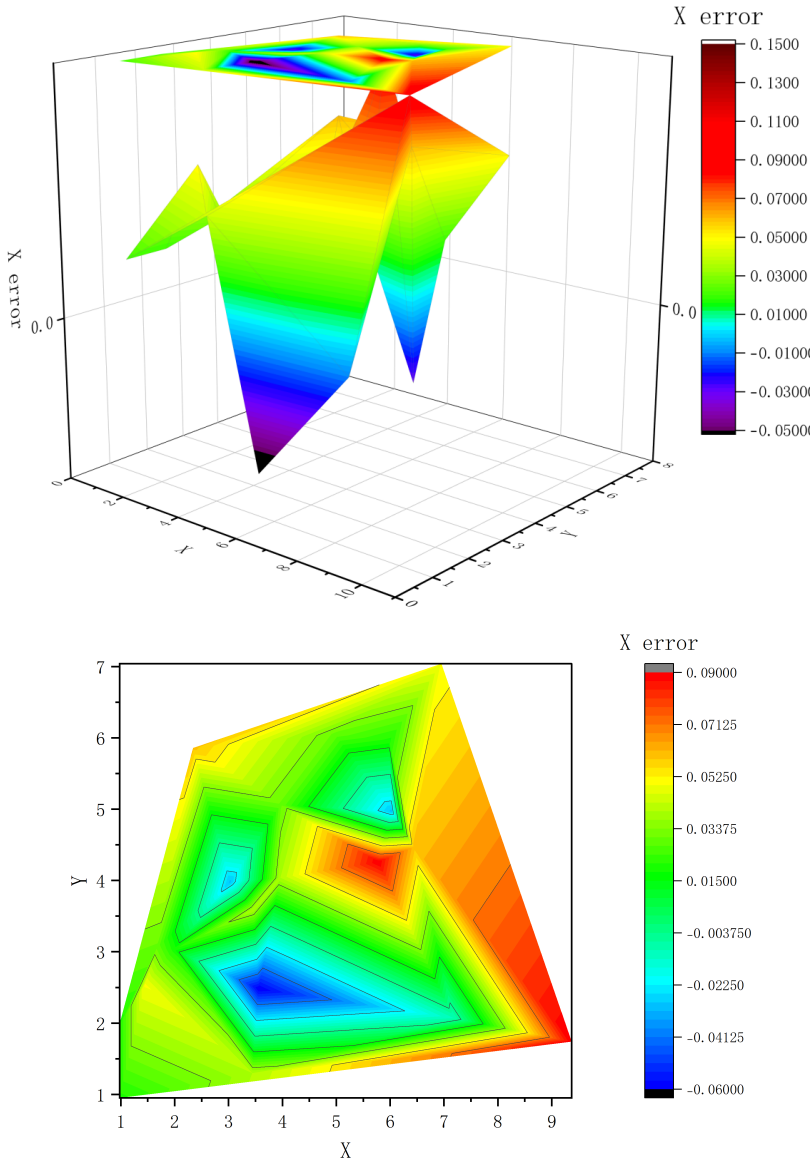


Figure 16. Error distribution image for X

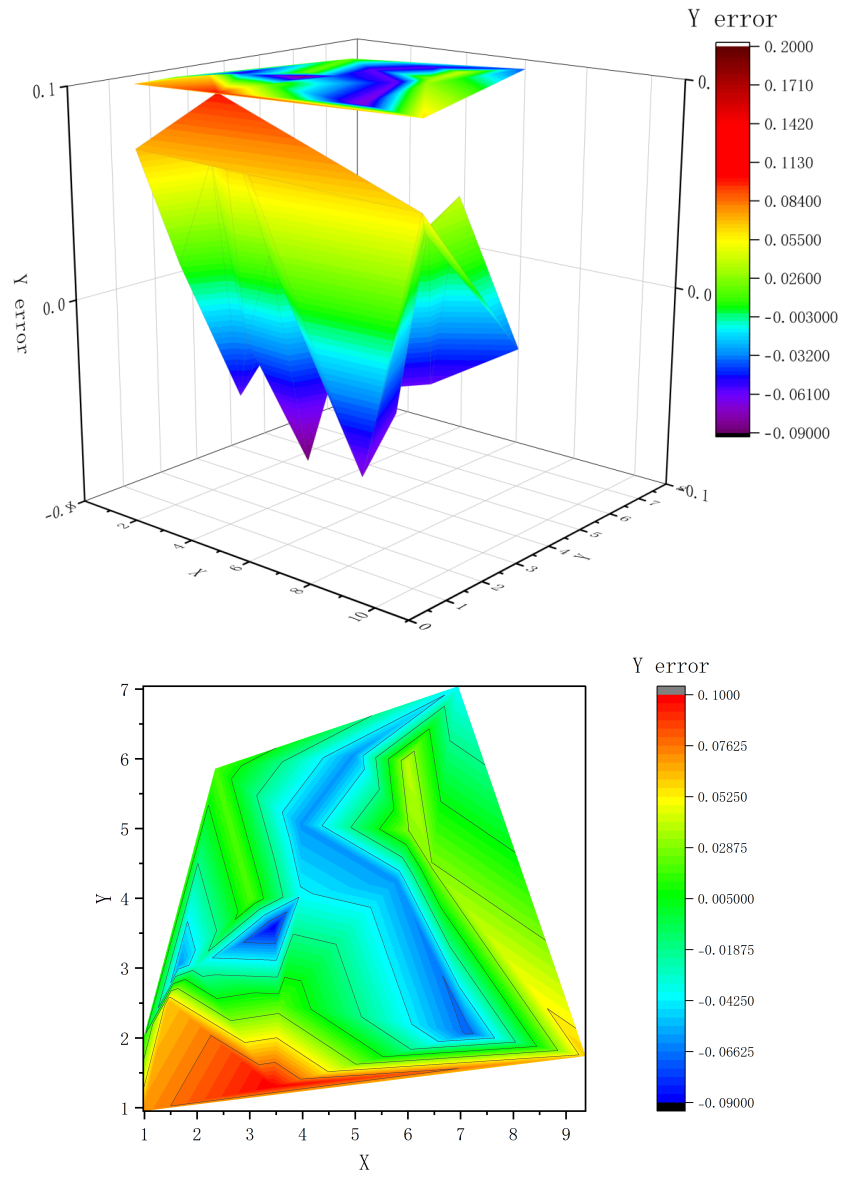


Figure 17. Error distribution image for Y

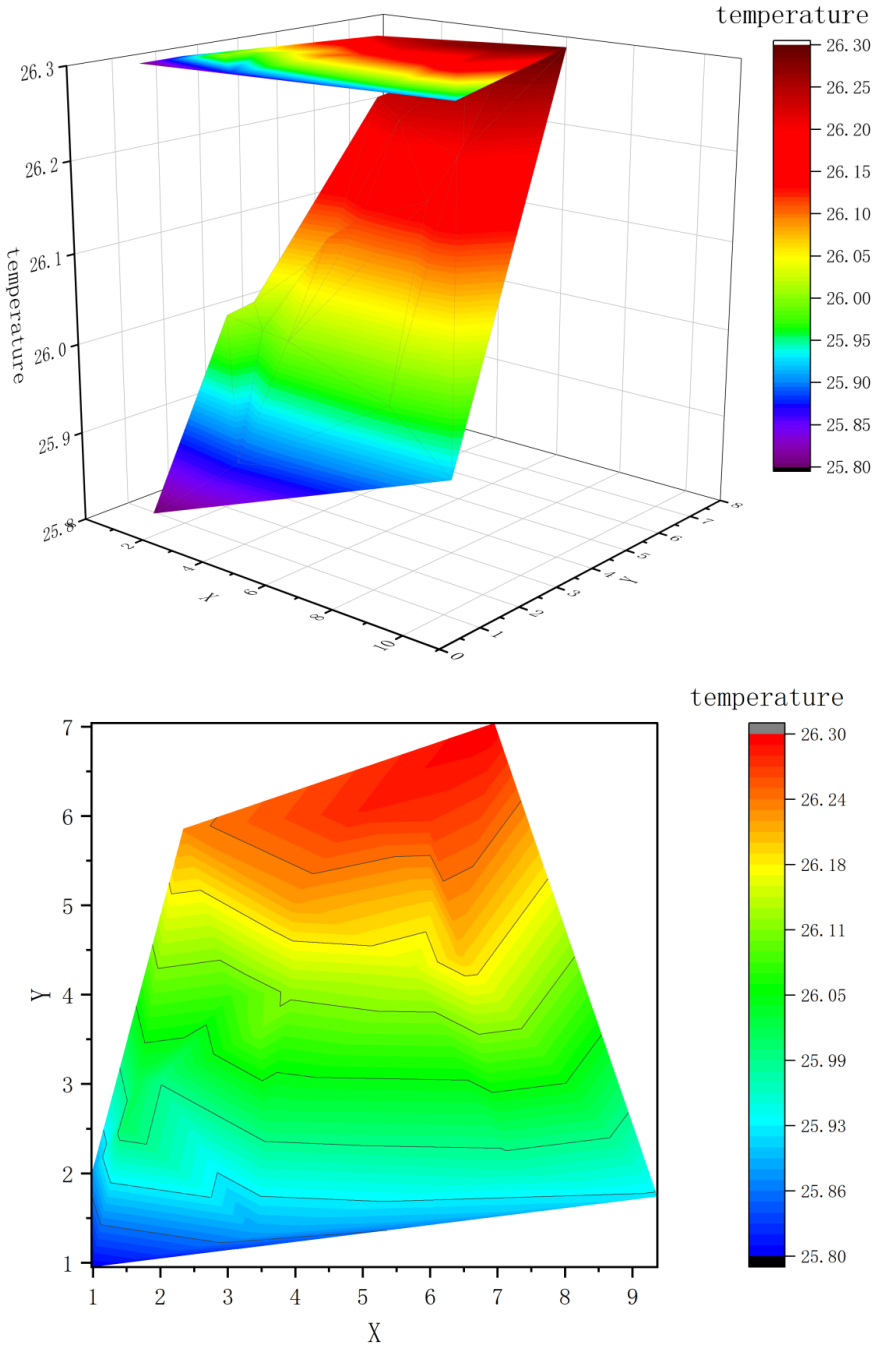
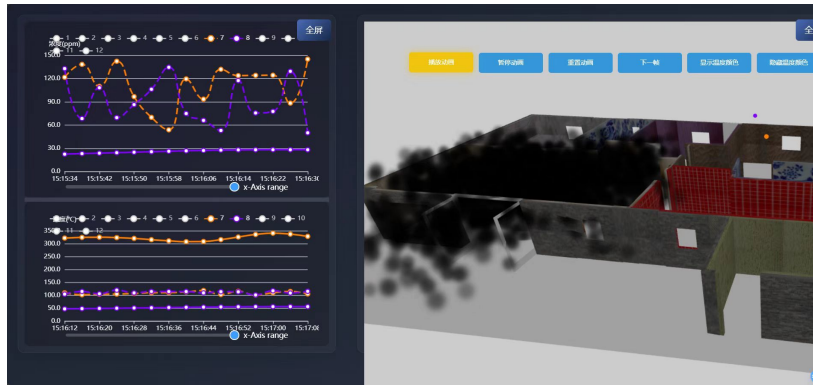
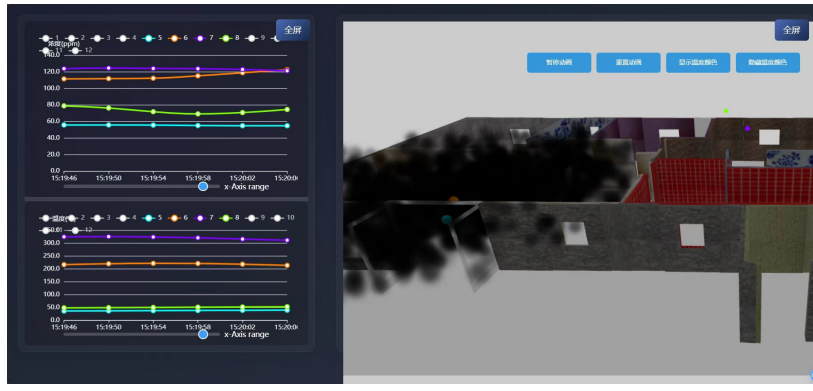


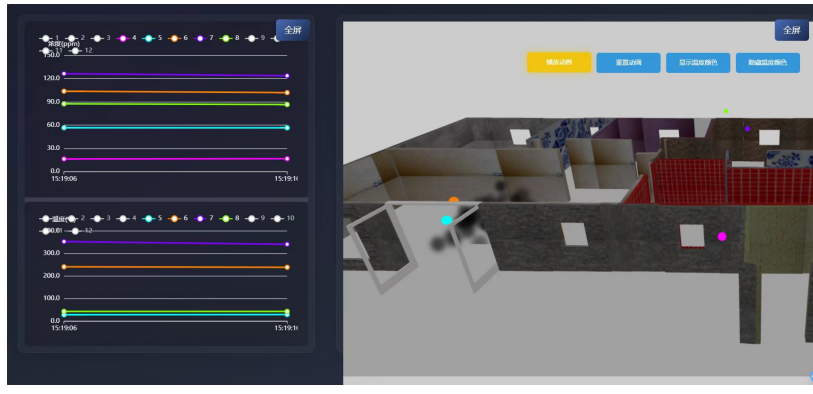
Figure 18. Temperature distribution map



a)



b)



c)

Figure 19. System visualization of temperature and smoke distribution field

and gas concentration. The positioning information serves as the foundation for 3D modeling of the fire scene, which enables data visualization, trend analysis, and optimization of rescue routes. Furthermore, the positioning results and real-time environmental parameters can be used to dynamically generate heatmaps of temperature and smoke on 2D or 3D maps. These maps can be integrated into web platforms or mobile terminals, allowing both the command center and frontline rescue personnel to simultaneously understand the fire situation.

6 CONCLUSIONS

This paper achieves centimeter-level indoor positioning through triangulation and model development, offering significant advantages over existing indoor positioning methods during fires. It operates effectively even when conventional sensors fail. The enhancements in positioning methods, along with the integration of the positioning device with temperature and smoke gas detection devices, were validated. This demonstrates its potential to support firefighting efforts better. In the event of failure of existing perception systems, the system's deployment and measurement capabilities can provide real-time rescue decision-making solutions, greatly assisting evacuation and rescue operations. By calculating and predicting temperature and smoke gas, a dynamically deployable, multi-node fire environment perception system is realized.

Further improvements can be made to the positioning device, such as using higher-precision sensors or adding more tags and selecting the four with the strongest signals in each area to reduce the impact of obstacles on signal accuracy. Once these enhancements are completed, the device can be applied in various scenarios. These include detecting toxic substances and harmful gas leaks in factories; monitoring temperature, humidity, and CO_2 concentration in smart agriculture; and performing real-time environmental anomaly detection (such as cable overheating) in smart cities. In the future, this device has the potential to evolve from a "post-disaster response" tool to a "pre-disaster warning" system across multiple fields, driving a comprehensive upgrade in intelligent safety management.

REFERENCES

[1] Shang, S.—Wang, L.: Overview of WiFi Fingerprinting-Based Indoor Positioning. IET Communications, Vol. 16, 2022, No. 7, pp. 725–733, doi: 10.1049/cmu2.12386.

[2] Liu, F.—Liu, J.—Yin, Y.—Wang, W.—Hu, D.—Chen, P.—Niu, Q.: Survey on WiFi-Based Indoor Positioning Techniques. IET Communications, Vol. 14, 2020, No. 9, pp. 1372–1383, doi: 10.1049/iet-com.2019.1059.

[3] Abbas, M.—Elhamshary, M.—Rizk, H.—Torki, M.—Youssef, M.: WiDeep: WiFi-Based Accurate and Robust Indoor Localization System Using Deep Learning. 2019 IEEE International Conference on Pervasive Computing and Communications (PerCom), 2019, pp. 1–10, doi: 10.1109/PERCOM.2019.8767421.

[4] Yu, K.—Wen, K.—Li, Y.—Zhang, S.—Zhang, K.: A Novel NLOS Mitigation Algorithm for UWB Localization in Harsh Indoor Environments. IEEE Transactions on Vehicular Technology, Vol. 68, 2019, No. 1, pp. 686–699, doi: 10.1109/TVT.2018.2883810.

[5] Sadowski, S.—Spachos, P.: RSSI-Based Indoor Localization with the Internet of Things. IEEE Access, Vol. 6, 2018, pp. 30149–30161, doi: 10.1109/ACCESS.2018.2843325.

[6] Wang, J.—Huangfu, Y.—Li, Z. et al.: Indoor Positioning Research Based on UWB Ranging Technology. Communication Power Supply Technology, Vol. 35, 2018, No. 5, pp. 50–53, doi: 10.19399/j.cnki.tpt.2018.05.019 (in Chinese).

[7] He, B.—Su, X.—Zhang, T.—Zhai, X.—Wang, B.—Dong, S.—Gao, J.: Design and Simulation of a Correction Compensation Triangulation Positioning Algorithm Based on RSSI. Agricultural Engineering, Vol. 14, 2024, No. 7, pp. 85–93, doi: 10.19998/j.cnki.2095-1795.2024.07.014 (in Chinese).

[8] Wang, J.—Yan, F.—Lu, X.—Feng, Y.: A Bluetooth Positioning Method Based on Least Squares Method. Computers and Network, Vol. 43, 2017, No. 19, pp. 72–74 (in Chinese).

[9] Li, Q.—Zhang, W.—Chen, J.: Comparison and Optimization of Numerical Fitting Methods for Fingerprint Curves. Modern Electronic Technology, Vol. 38, 2015, No. 24, pp. 27–30, doi: 10.16652/j.issn.1004-373x.2015.24.008 (in Chinese).

[10] Pan, H.—Qi, X.—Liu, M.—Liu, L.: An UWB-Based Indoor Coplanar Localization and Anchor Placement Optimization Method. Neural Computing and Applications, Vol. 34, 2022, No. 19, pp. 16845–16860, doi: 10.1007/s00521-022-07329-8.

[11] Li, Z.—Jiang, C.—Gu, X.—Xu, Y.—Zhou, F.—Cui, J.: Collaborative Positioning for Swarms: A Brief Survey of Vision, LiDAR and Wireless Sensors Based Methods. Defence Technology, Vol. 33, 2024, pp. 475–493, doi: 10.1016/j.dt.2023.05.013.

[12] Sui, X.—Ma, H.—Wang, C.—Chen, Z.—Shi, Z.—Gao, J.: Recognition of UWB NLOS in LiDAR Point Clouds and Indoor Fusion Positioning Algorithm. Journal of Geo-Information Science, Vol. 26, 2024, No. 12, pp. 2686–2700, doi: 10.12082/dqxxkx.2024.240442 (in Chinese).



Chongyu Wang is currently pursuing his B.Sc. degree in the field of measurement control technology and instruments from the Xiamen University, China. His current research interests include integrated positioning and embedded technology.



Xuhui Que received his B.Sc. degree in electrical engineering and automation from the Xiamen University, Xiamen, China, in 2022. He is currently pursuing his M.Sc. degree in instrumentation and measurement engineering at the Xiamen University, Xiamen, China. His current research interests include embedded systems, intelligent fire detection systems, wireless positioning, adaptive robotics algorithms, and WiFi-Mesh and UWB fusion positioning.



Defa Kong received his B.Sc. degree in mechanical engineering from the Yanshan University, China, in 2018. He is currently pursuing his M.Sc. degree in the Pen-Tung Sah Institute of Micro-Nano Science and Technology, Xiamen University, China. His current research interests include integrated positioning and embedded technology.



Juan Liu is Associate Professor of the Pen-Tung Sah Institute of Micro-Nano Science and Technology, Xiamen University; Member of the Laser Processing Committee of COS; Director of the Xiamen Micro-Electro-Mechanical Systems Society. Her primary research focuses on embedded systems, intelligent computing, laser robotic systems, micro-nano manufacturing systems, and related fields. She has presided over more than ten projects, including projects funded by the National Natural Science Foundation of China, sub-projects of national major research and development programs, and projects of the Provincial Natural Science Foundation. She has published over 40 papers, been granted 4 national invention patents, and won one Second Prize of Hubei Provincial Science and Technology Progress Award.